^{51}V Magic Angle Spinning NMR Spectroscopy of Keggin Anions [PV$_n$W$_{12-n}$O$_{40}$]$^{(3+n)-}$: Effect of Countercation and Vanadium Substitution on Fine Structure Constants

Wenlin Huang,[†] Louis Todaro,[‡] Glenn P. A. Yap,[†] Robert Beer,[§]
Lynn C. Francesconi,[‡] and Tatyana Polenova*,[†]

*Contribution from the Department of Chemistry and Biochemistry, University of Delaware,
Newark, Delaware 19716; Department of Chemistry, City University of New York-
Hunter College, 695 Park Avenue, New York, New York 10021; and Department of Chemistry,
Fordham University, 441 East Fordham Road, Bronx, New York 10458*

Received April 27, 2004; E-mail: tpolenov@chem.udel.edu

Abstract: Vanadium environments in Keggin oxopolytungstates were characterized by ^{51}V solid-state MAS NMR spectroscopy. (C$_4$H$_9$)$_4$N$^+$-, K$^+$-, Cs$^+$-, as well as mixed Na$^+$/Cs$^+$- salts of the mono-, di-, and trivanadium substituted oxotungstates, [VW$_{11}$O$_{40}$]$^{4-}$, [V$_2$W$_{10}$O$_{40}$]$^{5-}$, and [V$_3$W$_9$O$_{40}$]$^{6-}$, have been prepared as micro-crystalline and crystalline solids. Solid-state NMR spectra report on the local environment of the vanadium site in these Keggin ions via their anisotropic quadrupolar and chemical-shielding interactions. These ^{51}V fine structure constants in the solid state are determined by the number of vanadium atoms present in the oxoanion core. Surprisingly, the quadrupolar anisotropy tensors do not depend to any significant extent on the nature of the countercations. On the other hand, the chemical-shielding anisotropy tensors, as well as the isotropic chemical shifts, display large variations as a function of the cationic environment. This information can be used as a probe of the local cationic environment in the vanadium-substituted Keggin solids.

Introduction

The Keggin-type oxoanions are the most investigated family of polyoxometalates.[1,2] Polyoxomolybdates [PMo$_{12}$O$_{40}$]$^{3-}$ have been known since 1826,[3,4] and the first structure of a related polyoxotungstate [PW$_{12}$O$_{40}$]$^{3-}$ was reported by Keggin in 1933.[5] Interest in Keggin polyoxometalates has been growing in the recent years.[1,2] Relatively facile functionalization of the oxo-anion core [PM$_{12}$O$_{40}$]$^{3-}$, for example, by substituting different transition metals or rare earths metals (e.g., V(V), Cu(II), Ln(III), Eu(IV)) into one or more of the framework metal sites allows for fine-tuning of the electronic, photochemical, magnetic, and catalytic properties of Keggin compounds, making them attractive for the design of new materials for a variety of applications.[2,6,7]

Vanadium-containing Keggin polyoxometalates have received much attention due their catalytic activity, for example, in selective oxidations of hydrocarbons.[8-10] The presence of one or more vanadium(V) centers in the W(VI) or Mo(VI) oxoanion core has been shown to lead to greatly enhanced catalytic performance.[8-10] Recently, K. Nomiya and colleagues have studied toluene and nitrobenzene oxidation reactions catalyzed by vanadium-substituted polyoxomolybdates and polyoxotung-states.[9] They have shown that both the degree of vanadium substitution and the countercation environment of the vanadium center are key factors in determining the distribution of oxidation products and the catalyst stability.[9,10] It is thus of interest to investigate the role of both countercations and stoichiometry of the vanadium centers that affect the catalytic performance of these heteropolyoanions. Despite the fact that physical methods such as EPR, FTIR, Raman spectroscopy, and powder X-ray diffraction have been used to address these questions, the catalytic mechanism remains unclear.[8]

In this work, we investigated the local geometric and electronic environment of a series of vanadium-substituted Keggin oxopolyotungstates by ^{51}V solid-state Magic Angle Spinning NMR spectroscopy. We discuss the spectroscopic properties of a series of 10 molecules, (C$_4$H$_9$)$_4$N$^+$-, K$^+$-, Cs$^+$-, and mixed Na$^+$/Cs$^+$-salts of [VW$_{11}$O$_{40}$]$^{4-}$, [V$_2$W$_{10}$O$_{40}$]$^{5-}$, and [V$_3$W$_9$O$_{40}$]$^{6-}$, where the compounds have been prepared as

[†] University of Delaware.
[‡] City University of New York-Hunter College.
[§] Fordham University.
(1) Wassermann, K.; Palm, R.; Lunk, H.; Fuchs, J.; Steinfeldt, N.; Stosser, R. *Inorg. Chem.* **1995**, *34*, 5029−5036.
(2) Katsoulis, D. E. *Chem. Rev.* **1998**, *98*, 359−387.
(3) Pope, M. T.; Müller, A. *Angew. Chem., Int. Ed. Engl.* **1991**, *30*, 34−48.
(4) Berzelius, J. J. *Poggendorffs Ann. Phys. Chem.* **1826**, *6*, 369−380.
(5) Keggin, J. F. *Nature (London)* **1933**, *131*, 908.
(6) Kortz, U.; Mbomekalle, I. M.; Keita, B.; Nadjo, L.; Berthet, P. *Inorg. Chem.* **2002**, *41*, 6412−6416.
(7) Coronado, E.; Gómez-García, C. J. *Chem. Rev.* **1998**, *98*, 273−296.

(8) Inumaru, K.; Ono, A.; Kubo, H.; Misono, M. *J. Chem. Soc., Faraday Trans.* **1998**, *94*, 1765−1770.
(9) Nomiya, K.; Hashino, K.; Nemoto, Y.; Watanabe, M. *J. Mol. Catal. A* **2001**, *176*, 79−86.
(10) Nomiya, K.; Nemoto, Y.; Hasegawa, T.; Matsuoka, S. *J. Mol. Catal. A* **2000**, *152*, 55−68.

powder and diffraction quality crystals. We address the effect of the cation, the number of the vanadium atoms in the oxotungstate core, and the sample morphology on the ^{51}V solid-state NMR spectra. The solid-state NMR measurements presented herein, reveal that ^{51}V quadrupolar and chemical shielding anisotropies of these Keggin solids are determined by the number of vanadium atoms present in the oxoanion core. The ^{51}V chemical shielding anisotropy tensor components as well as the isotropic chemical shifts vary significantly as a function of the nature and geometry of the countercation. These results provide direct experimental evidence that the electronic properties of the oxoanion are modulated by the cationic environment and explain the previous observations concerning the dependence of chemical reactivities and thermal stabilities of Keggin polyoxometalates on the countercations.

Theoretical Considerations for ^{51}V Solid-State NMR Spectroscopy. Quadrupolar and Chemical Shielding Anisotropies. ^{51}V is a half-integer quadrupolar nucleus ($I = 7/2$) with high natural abundance (99.8%) and relatively high gyromagnetic ratio (Larmor frequency of 105.2 MHz at 9.4 T). The small quadrupolar moment allows direct observation of vanadium, and due to the favorable magnetic properties, small quantities of vanadium can be readily detected.

For half-integer spin nuclei, such as ^{51}V, the solid-state NMR spectra are dominated by a combination of the quadrupolar interaction (the interaction between the electric quadrupole moment of the nucleus and the electric field gradient on the nuclear site) and nuclear magnetic shielding anisotropy. The latter is observable in the NMR spectra via the symmetric part of the chemical shielding anisotropy (CSA) tensor,[11,12] and references therein. The different magnitudes and different symmetry properties of the quadrupolar and chemical shielding anisotropies allow these tensorial quantities to be extracted from a single spectrum, along with the mutual orientations of the quadrupolar and CSA tensors.[12] The total Hamiltonian in addition includes the dipolar and the radio frequency terms and can be expressed as follows:

$$\mathscr{H} = \mathscr{H}_{\text{Zeeman}} + \mathscr{H}_{\text{RF}} + \mathscr{H}_{\text{DIP}} + \mathscr{H}_{\text{Q}} + \mathscr{H}_{\text{CSA}} \quad (1)$$

The first three terms represent the Zeeman, the radio frequency field, and the dipolar interactions. The last two terms are the quadrupolar and CSA interactions, which dictate the spectral shape. They are conveniently expressed in a spherical tensor notation in terms of the spatial (R_{mn}) and spin (T_{mn}) variables:[13]

$$\mathscr{H}_{\text{Q}}^{(1)} = \frac{eQ}{4S(2S-1)} \cdot R_{20}^{\text{Q}} T_{20}^{\text{S}} = \omega_{\text{Q}}[3S_z^2 - S(S+1)] \quad (2)$$

$$\mathscr{H}_{\text{Q}}^{(2)} = \frac{C_{\text{Q}}}{\omega_0} \sum_{m \neq 0} \frac{R_{2m} R_{2-m}[T_{2m}, T_{2-m}]}{2m} \quad (3)$$

$$\mathscr{H}_{\text{CSA}} = -\gamma(R_{00}^{\text{CS}} T_{00}^{\text{S}} + R_{20}^{\text{CS}} T_{20}^{\text{S}}) = (\omega_{\text{CS}}^{\text{iso}} + \omega_{\text{CS}}^{\text{aniso}})S_Z \quad (4)$$

$\mathscr{H}_{\text{Q}}^{(1)}$ and $\mathscr{H}_{\text{Q}}^{(2)}$ are the first and second-order quadrupolar interaction. The quadrupolar and CSA tensor elements are

defined in a spherical harmonics basis set according to the standard notation:[14,15]

$$C_{\text{Q}} = \frac{eQV_{zz}}{h}; \quad \eta_{\text{Q}} = \frac{V_{yy} - V_{xx}}{V_{zz}}$$

$$\delta_\sigma = \delta_{zz} - {}^1/_2(\delta_{xx} + \delta_{yy}); \quad \eta_\sigma = \frac{\delta_{yy} - \delta_{xx}}{\delta_{zz} - \delta_{\text{iso}}};$$

$$\delta_{\text{iso}} = {}^1/_3(\delta_{xx} + \delta_{yy} + \delta_{zz}) \quad (5)$$

where C_{Q} is the quadrupolar coupling constant (in MHz); V_{xx}, V_{yy}, V_{zz} are the principal components of the electric field gradient (EFG) tensor, with $V_{zz} = eq$ being its largest principal component, and $|V_{zz}| \geq |V_{yy}| \geq |V_{xx}|$. C_{Q} defines the overall breadth of the spectral envelope. Q is the vanadium quadrupole moment (-0.052×10^{-28} V/m^2);[11] e is the electronic charge; h is the Planck constant. δ_{iso} is the isotropic chemical shift; δ_{xx}, δ_{yy}, and δ_{zz} are the principal components of the CSA tensor. δ_σ is the shielding anisotropy determining the breadth of the CSA tensor. η_{Q} and η_σ are the asymmetry parameters of the EFG and CSA tensors.

Upon spinning the solid powder sample at the Magic Angle (54.7°) the second-rank spatial components R_{20} of tensorial anisotropies of $\mathscr{H}_{\text{Q}}^{(1)}$ and $\mathscr{H}_{\text{CSA}}$ are efficiently averaged into a spinning sideband pattern while the fourth-rank terms of the $\mathscr{H}_{\text{Q}}^{(2)}$ are preserved, resulting in a characteristic second-order line shape.

Skibsted, Nielsen, Jacobsen, and their colleagues have previously demonstrated that the quadrupolar and the chemical shielding tensors, as well as their relative orientations can be extracted with high precision by detecting the complete manifold of spinning sidebands from the central and the satellite transitions and subsequently simulating the spectra.[12,16–21] These tensorial interactions can be further correlated with the structure and electronic properties at the vanadium site. Approximate estimates of the coordination geometries could be obtained from the quadrupolar coupling constant and the asymmetry parameter of the EFG tensor, using a simple electrostatic model.[22] According to the electrostatic model, the atoms in the first coordination sphere are treated as point charges, whose individual contributions to the electric field gradient on the central atom are combined to yield the net EFG tensor. This model is an oversimplification and cannot be relied on for precise quadrupolar interaction parameters, but it has been quite successful in predicting trends in homologous series of compounds, especially those containing bonds with significant ionic character.[16,17,22] In recent years, more rigorous quantum mechanical methods have been increasingly applied for calculations

(11) Smith, M. E.; van Eck, E. R. H. *Prog. NMR Spec.* **1999**, *34*, 159–201.
(12) Skibsted, J.; Nielsen, N. C.; Bildsøe, H.; Jacobsen, H. J. *Chem. Phys. Lett.* **1992**, *188*, 405–412.
(13) Frydman, L. *Annu. Rev. Phys. Chem.* **2001**, *52*, 463–498.

(14) Cohen, M. H.; Reif, F. *Solid State Physics* **1957**, *5*, 321–438.
(15) Schmidt-Rohr, K.; Spiess, H. W. *Multidimensional Solid-State NMR and Polymers*; Hartcourt Brace & Company: London, San Diego, New York, Boston, Sydney, Tokyo, 1999.
(16) Nielsen, U. G.; Jacobsen, H. J.; Skibsted, J. *Inorg. Chem.* **2000**, *39*, 2135–2145.
(17) Nielsen, U. G.; Jacobsen, H. J.; Skibsted, J. *J. Chem. Phys. B* **2001**, *105*, 420–429.
(18) Skibsted, J.; Jacobsen, C. J. H.; Jacobsen, H. J. *Inorg. Chem.* **1998**, *37*, 3083–3092.
(19) Skibsted, J.; Nielsen, N. C.; Bildsøe, H.; Jacobsen, H. J. *J. Magn. Reson.* **1991**, *95*, 88–117.
(20) Skibsted, J.; Jakobsen, H. J. *Inorg. Chem.* **1999**, *38*, 1806–1813.
(21) Jacobsen, H. J.; Skibsted, J.; Bildsøe, H.; Nielsen, N. C. *J. Magn. Reson.* **1989**, *85*, 173–180.
(22) Koller, H.; Engelhardt, G.; Kentgens, A. P. M.; Sauer, J. *J. Phys. Chem.* **1994**, *98*, 1544–1551.

of the EFG tensors, found experimentally by solid-state NMR, Mössbauer spectroscopy and other techniques.[23−30]

Experimental Section

Materials. All chemicals were obtained from Aldrich and used without further purification: sodium tungstate dihydrate ($Na_2WO_4 \cdot 2H_2O$), tungstophosphoric acid ($H_3PW_{12}O_{40} \cdot xH_2O$), vanadyl sulfate ($VOSO_4$), sodium metavanadate ($NaVO_3$), sulfuric acid, tetrabutyl-ammonium bromide (n-$C_4H_9)_4NBr$), cesium chloride, hydrochloric acid, glacial acetic acid.

α-$K_4[PVW_{11}O_{40}]$ (**I**) and α-1,2-$K_2H_3[V_2W_{10}O_{40}] \cdot 2CH_3OH \cdot 7H_2O$ (**V**), and α-1,2,3-$K_6[PV_3W_9O_{40}]$ (**VIII**) have been synthesized according to the literature protocols.[31] Either (n-$C_4H_9)_4NBr$ or CsCl, or NaCl/CsCl was used in the last step of the synthesis to obtain the corresponding salts of the α-vanadoundecatungstophosphate: ((n-$C_4H_9)_4N)_4[PVW_{11}O_{40}]$ (**II**), $Cs_4PVW_{11}O_{40}$ (**III**), $Na_2Cs_2PVW_{11}O_{40}$ (**IV**), α-1,2-$Cs_5PV_2W_{10}O_{40}$ (**VII**), or α-1,2,3-$Cs_6PV_3W_9O_{40}$ (**X**). Tetrabutylammonium α-divanado-decatungstophosphate (α-1,2-((n-$C_4H_9)_4N)_5[PV_2W_{10}O_{40}]$ (**VI**)) and tetrabutylammonium α-trivanadononatungstophosphate (α-1,2,3-[(n-$C_4H_9)_4N]_6$-$[PV_3W_9O_{40}]$ (**IX**)) was obtained by adding (n-$C_4H_9)_4NBr$ into the α-1,2-$K_5[PV_2W_{10}O_{40}]$ solution at acidic conditions (pH = 2). Compounds **II**, **V**, **VI** were prepared as a microcrystalline powder or diffraction-quality crystals. Despite repeated crystallization attempts, **I**, **III**, and **IV** consistently form powders. Their powder samples were prepared by fast precipitation from concentrated anion solutions using an excess of the corresponding countercation. The trivanadium substituted Keggin anions α-1,2,3-$K_6[PV_3W_{10}O_{40}]$ (**VIII**), α-1,2,3-((n-$C_4H_9)_4N)_6[PV_3W_9O_{40}]$ (**IX**), and α-1,2,3-$Cs_6[PV_3W_9O_{40}]$ (**X**) were prepared as powders.

Crystal Structure of $K_2H_3[V_2W_{10}O_{40}] \cdot 2CH_3OH \cdot 7H_2O$. Diffraction quality single crystals of **V** were prepared by gradually cooling a saturated aqueous solution from 80 °C to 4 °C at pH = 2. The intensity data for **V** were measured on a Bruker−Nonius KappaCCD diffractometer (graphite-monochromated Mo Kα radiation, ϕ−ω scans). Of the 11 239 independent reflections for θ < 27.45°, 9701 were considered observed [$I > 2.0\sigma(I)$]. The structure of **V** was solved with SHELXS-97 and refined by full-matrix least squares on F^2 with SHELXL-97.[32] In the crystal, the various heavy-atom sites were occupied by both tungsten and vanadium atoms in an approximate ratio of 10 to 2, respectively: so the twelve occupancy factors of the so-called tungsten atoms refined to partial occupancies. In the final refinement, the non-hydrogen atoms were refined anisotropically. The hydrogen atoms of the solvent atoms were not included in the structure-factor calculations. The final difference map peaks (<1.10 e Å^{-3}) were near the tungsten/vanadium atoms.

Crystal Structure of $[(n$-$C_4H_9)_4N]_4[PVW_{11}O_{40}]$ (II) and $[(n$-$C_4H_9)_4N]_5[PV_2W_{10}O_{40}]$ (VI). Crystals of **II** and **VI** were prepared by gradual cooling of hot saturated solutions in N,N-dimethylformamide solvent. Suitable crystals were selected, sectioned, mounted with Paratone oil on glass fibers and flash-cooled to the data collection temperature. Diffraction data were collected on a Bruker AXS SMART

APEX diffractometer using Mo kα radiation ($\lambda = 0.7173$ Å). Unit cell parameters were obtained from 60 data frames, 0.3° ω, from three different sections of the Ewald sphere. Systematic absences in the diffraction data and unit cell parameters were consistent with space groups $I4$ (No. 79), I-4 (No. 82), $I4/m$ (No. 87), $I422$ (No. 97), $I4mm$ (No. 107), I-42m (No. 121) and $I4/mmm$ (No. 139) for **II** and $I23$ (No. 197), $I2_13$ (No. 199), Im-3 (No. 204), $I432$ (No. 211), I-43m (No. 217) and Im-3m (No. 229) for **VI**. The cubic crystal system for **VI** was confirmed by polarized light microscopy. After an exhaustive exploration of the space group options, only the reported space groups yielded reasonable connectivity and computationally stable results of refinement. The data sets were treated with SADABS absorption corrections based on redundant data. Each data set was treated as racemic twin data with a roughly 50/50 distribution. The structures were solved using direct methods and refined by full-matrix least squares on F^2. Atom identities in the anions were chosen as best-fit models within the range of known possible atoms to represent irresolvable heavy atom disorder. The severely disordered cations were refined isotropically with common displacement parameters for the carbon atoms and with restrained equal N−C bond distances, C_1−C_2 bond distances and C_1−C_3 interatomic separations. The occupancy of the cation atoms in **VI** are based on noncrystallographic information. All non-hydrogen anion atoms were refined with anisotropic displacement parameters. All hydrogen atoms on the ammonium cations were treated as idealized contributions. Structure factors and anomalous dispersion coefficients are contained in the SHELXTL 6.12 program library.[32]

FTIR Spectroscopy. FTIR spectra of **I**−**VI** were acquired using a Nicolet Magna 560 FTIR spectrometer with a liquid nitrogen cooled MCT detector. Infrared spectra were recorded at room temperature with 4 cm^{-1} resolution and 32 scans per experiment.

Solution NMR Spectroscopy. ^{51}V and ^{31}P solution NMR spectra were acquired at 9.4T on a JEOL GSX-400 spectrometer equipped with Delta data system. The ^{51}V and ^{31}P resonance frequencies were 105.12 and 161.87 MHz, respectively. All spectra were acquired using a 5 mm broadband probe. ^{51}V spectra were acquired using a 5.8 μs (30°) single pulse; the ^{31}P spectra were acquired with a 15 μs (90°) single pulse. 2048 complex FID points were collected for ^{51}V, the total acquisition time of 48.7 ms, and the recycle delay of 500 ms. For ^{31}P, a recycle delay of 2 s was used. The spectra were processed with 2 Hz exponential line broadening; no zero filling was applied. The isotropic chemical shifts are reported relative to the neat $VOCl_3$ sample and H_3-PO_4, used as the external reference.

Solid-State NMR Spectroscopy. ^{51}V solid-state NMR spectra were acquired at 105.2 MHz (9.4 T) on a Tecmag Discovery spectrometer using a 4 mm Doty XC4 MAS probe. Spectra were recorded using 8−16 mg of sample. For each of the compounds, spectra at several different spinning speeds ranging between 4 and 17 kHz were acquired. The spinning speed was controlled to within ±5 Hz. The Magic Angle was adjusted using $NaNO_3$ (by detecting the ^{23}Na MAS signal). A single 1 μs pulse ($\gamma H_1/2\pi \approx 80$ kHz) was employed to excite the central and the satellite transitions; 1 s recycle delays were used. The spectral widths were 1.25 MHz, and 4096 complex data points were acquired. The data were processed by linear prediction of the first 66 points to suppress the baseline distortions, followed by Fourier transformation and baseline correction using the MestRe−C23 NMR data processing software.[33] Isotropic chemical shifts are reported with respect to neat $VOCl_3$, whose ^{51}V spectrum was recorded and used as an external reference.

Additional data sets for **I**−**III**, **V**, and **VI** were acquired at 131.371 MHz (11.74 T) on a Varian Inova spectrometer using a 4 mm Doty XC4 MAS probe. The spinning speeds, the data acquisition and processing parameters were identical to those at 9.4 T.

Simulations of the NMR Spectra. Numerical simulations of the experimental ^{51}V solid-state NMR spectra were performed on a 1.1

(23) Marichal, C.; Kempf, J.-Y.; Maigret, B.; Hirschinger, J. *Solid State NMR* **1997**, *8*, 33−46.
(24) Bryant, P. L.; Harwell, C. R.; Wu, K.; Fronczek, F. R.; Hall, R. W.; Butler, L. G. *J. Phys. Chem. A* **1999**, *103*, 5246−5252.
(25) Moore, E. A.; Johnson, C.; Mortimer, M.; Wigglesworth, C. *Phys. Chem. Chem. Phys.* **2000**, *2*, 1325−1331.
(26) Tsvyashchenko, A. V.; Fomicheva, L. N.; Magnitskaya, M. V.; Shirani, E. N.; Brudanin, V. B.; Filossofov, D. V.; Kochetov, O. I.; Lebedev, N. A.; Novgorodov, A. F.; Salamatin, A. V.; Korolev, N. A.; Velichkov, A. I.; Timkin, V. V.; Menushenkov, A. P.; Kuznetsov, A. V.; Shabanov, V. M.; Akselrod, Z. Z. *Solid State Commun.* **2001**, *119*, 153−158.
(27) Blaha, P.; Schwartz, K.; Herzig, P. *Phys. Rev. Lett.* **1985**, *54*, 1192−1195.
(28) Bryce, D. L.; Wasylishen, R. E. *Phys. Chem. Chem. Phys.* **2002**, *4*, 3591−3600.
(29) Munro, O. Q.; Shabalala, S. C.; Brown, N. J. *Inorg. Chem.* **2001**, *40*, 3303−3317.
(30) Pooransingh, N. P. E.; Ebel, M.; Jantzen, S.; Rehder, D.; Polenova, T. *Inorg. Chem.* **2003**, *42*, 1256−1266.
(31) Domaille, P. J. *J. Am. Chem. Soc.* **1984**, *106*, 7677−7687.
(32) Sheldrick, G. *SHELXTL*; Bruker-AXS: Madison, WI, 2001.

(33) Cobas, J.; Cruces, J.; Sardina, F. J. *MestRe−C: Magnetic Resonance Companion*; Departamento de Quimica Organica, Facultat de Quimica, Universidad de Santiago de Compostela, Spain, 2000.

Table 1. Crystal Data and Structure Refinement for $[(n\text{-}C_4H_9)_4N]_4[PVW_{11}O_{40}]$ (**II**), $\alpha\text{-}1,2\text{-}K_2H_3[V_2W_{10}O_{40}]\cdot2CH_3OH\cdot7H_2O$ (**V**), and $[(n\text{-}C_4H_9)_4N]_5[PV_2W_{10}O_{40}]$ (**VI**)

	II	V	VI
formula	$C_{64}H_{144}N_4O_{40}PVW_{11}$	$C_2H_{23}KO_{49}PV_2W_{10}$	$C_{64}H_{145}N_4O_{40}PV_2W_{10}$
fw	3714.09	2925.73	3582.12
T (K)	150(2)	295	150(2)
crystal system	tetragonal	trigonal	cubic
space group	$I\text{-}4$	$P3_2$	$I\text{-}43m$
a (Å)	18.6299(7)	19.057(3)	17.588(3)
b (Å)	18.6299(7)	19.057(3)	17.588(3)
c (Å)	14.3535(10)	12.505 (3)	17.588(3)
α (°)	90	90	90
β (°)	90	90	90
γ (°)	90	120	90
V (Å^3)	49817(4)	3933.0(11)	5440.7(13)
ρ (g/cm^3) (calc.)	2.476	3.706	2.187
Z, Z'	8, 0.25	3, 1	48, 0.041 667
μ(Mo Kα) (mm^{-1})	12.823	22.474	10.771
crystal size (mm)	$0.30 \times 0.28 \times 0.25$	$0.03 \times 0.05 \times 0.50$	$0.40 \times 0.30 \times 0.30$
max θ for data collection (°)	28.28	27.45	28.06
reflns unique/observed	15371/5744	11239/9701	16645/1227
no. of variables	174	629	82
min/max transmission (%)	10.31/12.89	3.14/ 60.34	7.99/11.42
$R(F)$ (%)^a	4.29	6.09	3.44
$R_w(F^2)$ (%)^a	11.50	11.18	9.87
largest diff peak, hole, (e/Å^3)	1.84, -1.28	1.06, -1.10	0.96, -3.70

^{a} Quantity minimized $= R(wF^2) = \{\sum[w(F_o^2 - F_c^2)^2]/\sum(wF_o^2)^2\}^{1/2}$: $R(F) = \sum\Delta/\sum(F_o)$, $\Delta = |(F_o - F_c)|$: $w = [\sigma^2(F_o^2) + (aP)^2 + bP]^{-1}$:$P = [2F_c^2 + \text{Max}(F_o,0)]/3$.

GHz Pentium-4 PC under Linux environment using the SIMPSON software package.[34] The combined effect of the quadrupolar interaction to second order and chemical shielding anisotropy was taken into account in the simulations. The seven independent parameters describing the quadrupolar and CSA tensor anisotropies (C_Q, η_Q, δ_σ, and η_σ) and the relative tensor orientations (the Euler angles α, β, and γ) were obtained by the least-squares fitting of the simulated and experimental sideband intensities using a home-written program in Mathematica 5.0 (Wolfram, Inc.). The quality factor of the probe (Q) has been taken into account in the simulations.

Calculation of Atomic Charges. Atomic charges in $[(n\text{-}C_4H_9)_4N]^+$ were calculated quantum mechanically using density functional theory implemented in Gaussian98.[35] Becke's three-parameter hybrid B3LYP functional and 6-31G basis set were used.[36] Calculations were performed the IBM pSeries 690 system at the National Center for Supercomputing Applications (NCSA).

Single-point calculation was conducted with the TBA geometry derived from the experimental X-ray structures. Both Mulliken charges and those derived from the natural population analysis were considered.

Results and Discussion

Single-Crystal X-ray Diffraction of $\alpha\text{-}1,2\text{-}K_2H_3[PV_2W_{10}O_{40}]\cdot 2CH_3OH\cdot7H_2O$ (V). The potassium salt of divanadium substituted Keggin polyoxotungstate crystallizes in the trigonal space group $P3_2$ with one oxoanion molecule per unit cell. Positional disorder with respect to the vanadium atom(s) is

present in the structures, which is quite common for the substituted heteropoly anions.[37-39] The X-ray data can be explained assuming statistical distribution of vanadium atoms in the tungstate framework. The stoichiometry of substituted heteropoly anions in the X-ray crystal structures can only be inferred from the relative site occupancies. The structure of **V** refined with the relative W:V site occupancies of 5:1, in agreement with the expected stoichiometry.

Electron densities corresponding only to three K$^+$ cations per one $PV_2W_{10}O_{40}^{5-}$ anion could be identified. We therefore conclude that three additional protons are present in the structure to balance the overall charge of the anion. This is also consistent with the fact that **V** was prepared under acidic conditions (pH 2.0). The crystal data and structure refinement parameters are given in Table 1.

In Figure 1, the packing diagram is shown. One of the K$^+$ cations is at a distance of 2.83 Å from the bridging oxygen on one oxoanion, whereas the second K$^+$ is at 2.73 Å from the terminal oxo ligands on two adjacent POMs. Fourteen coordination waters and one molecule of methanol were identified in the crystal structure.

Single-Crystal X-ray Diffraction of $[(n\text{-}C_4H_9)_4N]_4$-$[PVW_{11}O_{40}]$ (II) and $[(n\text{-}C_4H_9)_4N]_4H[PV_2W_{10}O_{40}]$ (VI). The n-tetrabutylammonium salts of mono- and di- vanadium substituted Keggin polyoxotungstates crystallize in cubic $I\text{-}4$ and $I\text{-}43m$ space groups, respectively, with two oxoanion molecules, and eight n-tetrabutylammonium cations per unit cell. The crystal data and structure refinement parameters are given in Table 1.

Similar to **V**, positional disorder with respect to vanadium atoms was observed in the crystal structure of **II** and **VI**. Since

(34) Bak, M.; Rasmussen, J. T.; Nielsen, N. C. *J. Magn. Reson.* **2000**, *147*, 296−330.
(35) Frisch, M. J.; Trucks, G. W.; Schlegel, H. B.; Scuseria, G. E.; Robb, M. A.; Cheeseman, J. R.; Zakrzewski, V. G.; Montgomery, J. A. J.; Stratmann, R. E.; Burant, J. C.; Dapprich, S.; Millam, J. M.; Daniels, A. D.; Kudin, K. N.; Strain, M. C.; Farkas, O.; Tomasi, J.; Barone, V.; Cossi, M.; Cammi, R.; Mennucci, B.; Pomelli, C.; Adamo, C.; Clifford, S.; Ochterski, J.; Petersson, G. A.; Ayala, P. Y.; Cui, Q.; Morokuma, K.; Salvador, P.; Dannenberg, J. J.; Malick, D. K.; Rabuck, A. D.; Raghavachari, K.; Foresman, J. B.; Cioslowski, J.; Ortiz, J. V.; Baboul, A. G.; Stefanov, B. B.; Liu, G.; Liashenko, A.; Piskorz, P.; Komaromi, I.; Gomperts, R.; Martin, R. L.; Fox, D. J.; Keith, T.; Al-Laham, M. A.; Peng, C. Y.; Nanayakkara, A.; Challacombe, M.; Gill, P. M. W.; Johnson, B.; Chen, W.; Wong, M. W.; Andres, J. L.; Gonzalez, C.; Head-Gordon, M.; Replogle, E. S.; Pople, J. A. *Gaussian 98*; Revision A.1x ed.; Gaussian, Inc.: Pittsburgh, PA, 2001.
(36) Becke, A. D. *J. Chem. Phys.* **1993**, *98*, 5648−5652.
(37) Klevtsova, R. F.; Yurchenko, E. N.; Glinskaya, L. A.; Derkach, I. V.; Markes-Rios, A. *J. Struct. Chem.* **1988**, *29*, 418−421.
(38) Nishikawa, K.; Kobayashi, A.; Sasaki, Y. *Bull. Chem. Soc. Jpn.* **1975**, *48*, 889−892.
(39) Luo, Q.-H.; Howell, R.; Dankova, M.; Bartis, J.; Williams, C. W.; Horrocks, W. D., Jr.; Young, V. G., Jr.; Rheingold, A. L.; Francesconi, L. C.; Antonio, M. R. *Inorg. Chem.* **2001**, *40*, 1894−1901.
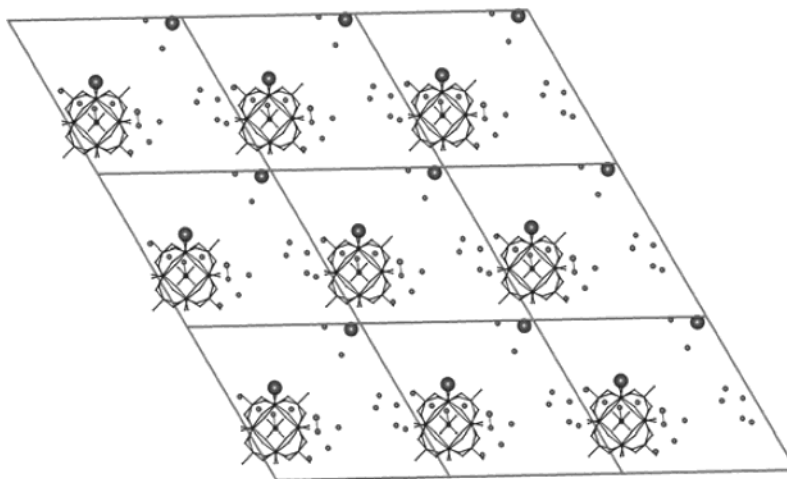
Figure 1. Coordination environment of α-1,2-K$_2$H$_3$[PV$_2$W$_{10}$O$_{40}$]·2CH$_3$OH·7H$_2$O (**V**). View down the crystallographic *a* axis to indicate packing of the K$^+$ countercations and solvent molecules. Vanadium atoms display positional disorder within the crystal lattice. The anion is shown in a wireframe representation. The O atoms of the solvent are depicted as small spheres, the K$^+$ cations are shown as large spheres, and the protons are omitted. One of the K$^+$ cations (shown in light gray) is at a distance of 2.83 Å from the bridging oxygen on one POM molecule, while the second K$^+$ (shown in dark gray) is at 2.73 Å from the terminal oxo ligands on two adjacent polyoxometalates. The crystal structure suggests weak electrostatic interactions between the K$^+$ cations and the vanadium atoms in the polyoxotungstate clusters.

the crystal symmetry is higher than the molecular symmetry and the heavy atom positions are disordered, we employed the crystal structures of **II** and **VI** only to infer the overall countercation arrangement in these solids. The stoichiometry of the complexes was confirmed using NMR ^{31}P and ^{51}V chemical shifts, as well as the FTIR vibrational frequencies (as discussed in the previous section).

In Figure 2, the coordination environments are shown for **II** and **VI**. In both compounds, each POM anion is surrounded by eight [(*n*-C$_4$H$_9$)$_4$N]$^+$ cations resulting in a pseudo-octahedral environment for the anion. As the electron density maps of **VI** did not indicate other cationic species, an additional H$^+$ is likely to be present in the structure for charge neutrality, which is also consistent with the acidic conditions (pH = 2) used in the preparation of the complex.

These results suggest that coordination environments in Keggin polyoxoanions do not differ significantly for mono- and di-vanadium substituted molecules, and depend only on the nature of the countercation. We observed similar behavior in the vanadium-substituted Lindqvist hexatungstates.[40]

FT-IR Spectroscopy of Vanadium-Substituted Keggin Oxotungstates. Vanadium-substituted Keggin anions display characteristic FT-IR bands in the region of 1060−1100 cm^{-1} giving rise to the additional V−O(terminal) stretch vibration whose frequency appears close to the P−O stretch vibration of the tetrahedral PO$_4$ unit in the oxoanion core. The combination of these vibrations yields a distinct multiplet structure, which depends on the degree of vanadium substitution (doublet for mono-vanadium, triplet for di-vanadium, and triplet with distinct intensity ratios for tri-V-substituted oxotungstates). The FT-IR spectra are consistent with the bands associated with mono (**I**−**IV**), di (**V**−**VII**), and tri (**VIII**−**X**) substituted anions. The vibrational frequencies are presented in Table 2; the detailed discussion will be reported elsewhere.

Solution NMR Characterization of the Keggin Oxoanions I, II, V, and VI. We have acquired multinuclear (^{31}P and ^{51}V) solution NMR spectra for four mono- and di- vanadium

substituted Keggin anions under investigation. The solution chemical shifts are compiled in Table 3. For **I** and **V**, ^{31}P and ^{51}V solution chemical shifts have been reported previously, and our results are in good agreement with the literature data.[31] The di-vanadium substituted complexes **V** and **VI** represent individual positional isomers rather than a mixture of stereoisomers, as is evidenced by a single peak in the ^{51}V solution NMR spectra.[31] The tetrabutylammonium salts of mono- and di-vanadium substituted **II** and **VI** exhibit different chemical shifts in solution (^{51}V and ^{31}P), attesting to the different degree of vanadium substitution in these compounds.

^{51}V Solid-State NMR Magic Angle Spinning Spectroscopy: Isotropic Chemical Shifts and Anisotropic Line Shapes. The ^{51}V MAS solid-state NMR spectra of **I**−**IV** acquired at 9.7 T and a spinning speed of 15 kHz are presented in Figure 3; the corresponding spectra of **V**−**VI** are displayed in Figure 4. The isotropic chemical shifts are compiled in Table 3. The second-order quadrupole induced shifts were taken into account as a correction to the experimentally observed isotropic sideband according to literature:[41]

$$\delta_{observed} - \delta_{iso} = \frac{-3*10^6(e^2qQ/h)^2[I(I+1) - 9m(m-1) - 3][1 + \eta^2/3]}{40(\nu_0^2)[I(2I-1)]^2} \quad (6)$$

where (e^2qQ/h) is the quadrupolar coupling constant (in MHz), *I* is the spin number; $I = 7/2$ for ^{51}V; *m* is the magnetic spin number ($m = 1/2$ for the central transition), η is the asymmetry of the CSA tensor, ν_0 is the resonance frequency of the ^{51}V nucleus (105.2 MHz at 9.4T). For the compounds reported in this work, these upfield shifts ranged from −0.1 to −2 ppm.

^{51}V solution and solid-state isotropic chemical shifts differ by several ppm, suggesting that the local environments of the vanadium nucleus are different. Similar behavior was observed previously in Lindqvist polyoxometalates,[40] as well as bioinorganic oxovanadium(V) complexes.[30] As observed previously,[31] di- and tri-vanadium derivatives exhibit a single peak

(40) Huang, W.; Todaro, L.; Francesconi, L. C.; Polenova, T. *J. Am. Chem. Soc.* **2003**, *125*, 5928−5938.

(41) Kundla, E.; Samoson, A.; Lipmaa, E. *Chem. Phys. Lett.* **1981**, *83*, 229.
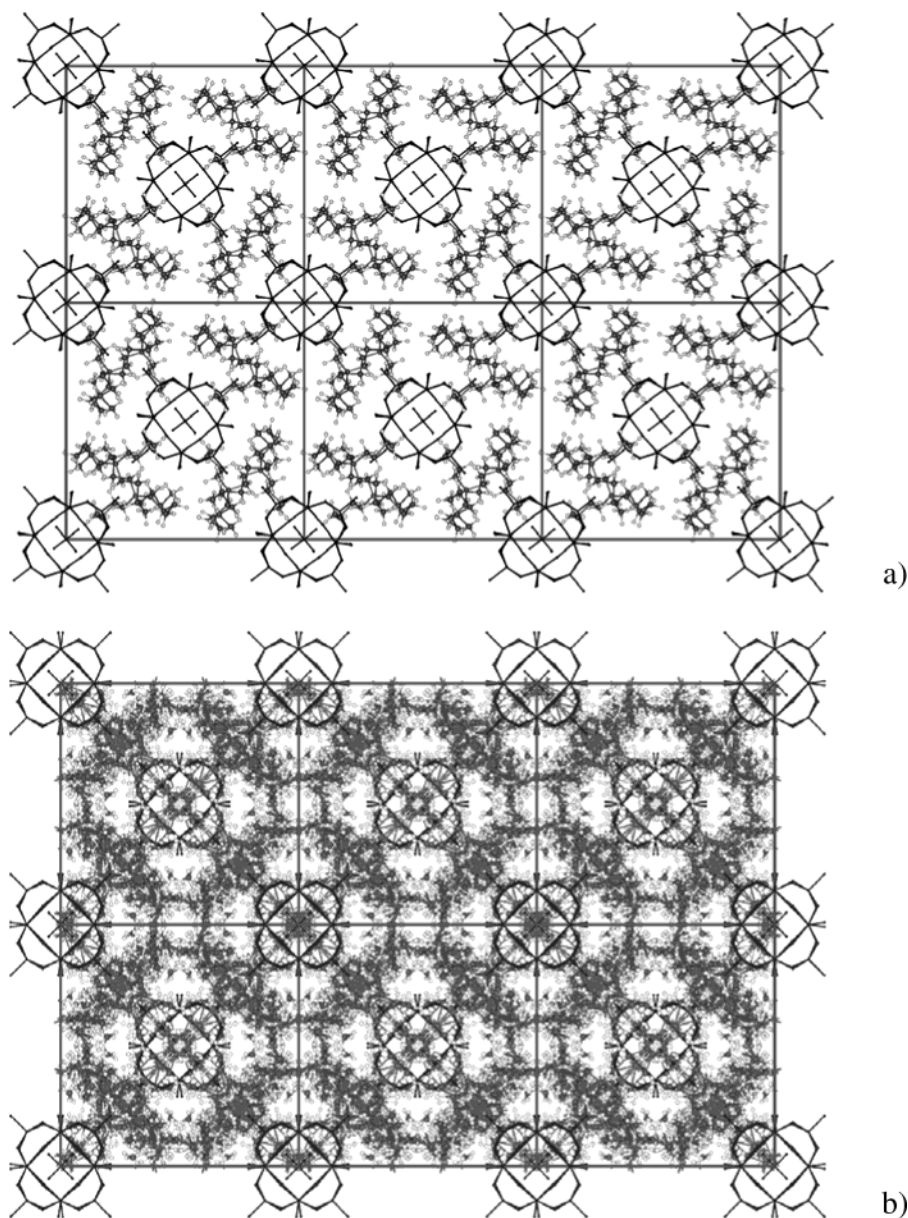
Figure 2. Coordination environments and unit cells of (a) $[(n\text{-}C_4H_9)_4N]_4[PVW_{11}O_{40}]$ (**II**) and (b) $[(n\text{-}C_4H_9)_4N]_4H[PV_2W_{10}O_{40}]$ (**VI**). View down the crystallographic **c** axis to indicate packing of the $[(n\text{-}C_4H_9)_4N]^+$ countercations. The vanadium atoms display positional disorder within the crystal lattice; In both **II** and **IV**, each anion is surrounded by eight cation molecules. An additional H^+ is likely to be present in the structure of **VI** for charge neutrality; however, it is not revealed in the electron density and is thus not shown here. The anion is shown in a wireframe representation. $[(n\text{-}C_4H_9)_4N]^+$ is depicted in a ball-and-stick representation.

Table 2. Experimental FTIR Parameters for Vanadium-Substituted Keggin Polyoxotungstate Solids **I**−**X** (KBr pellet) (characteristic V−O and P−O stretching frequencies are given in bold)

compd	experimental infrared frequencies
I $K_4PVW_{11}O_{40}$	1618, (**1103, 1082**),[a] 990, 885, 789, 601, 526
II $[(n\text{-}C_4H_9)_4N]_4PVW_{11}O_{40}$	2962, 2873, 1485, 1386, (**1100, 1071**),[a] 963, 891, 812, 601, 526
III $Cs_4PVW_{11}O_{40}$	
IV $[Na_xCs_{4-x}]PVW_{11}O_{40}$	1622, (**1100, 1072**),[a] 973, 908, 803, 598, 512
V $\alpha\text{-}1,2\text{-}K_2H_3[PV_2W_{10}O_{40}]\cdot2CH_3OH\cdot7H_2O$	1637, (**1100, 1079, 1062**),[b] 966, 898, 792, 601, 509
VI $\alpha\text{-}1,2\text{-}[(n\text{-}C_4H_9)_4N]_5PV_2W_{10}O_4$	2996, 2877, 1485, 1383, (**1103, 1082, 1061**),[b] 963, 894, 806, 598, 523
VII $\alpha\text{-}1,2\text{-}Cs_5PV_2W_{10}O_{40}$	2980, 1635, (**1096, 1079, 1055**),[b] 980, 874, 792, 597, 509
VIII $\alpha\text{-}1,2,3\text{-}K_6PV_3W_9O_{40}$	3741, 3481, 2925, 1625, (**1089, 1059**),[c] 960, 871, 796, 625, 526
IX $\alpha\text{-}1,2,3\text{-}[(n\text{-}C_4H_9)_4N]_6PV_3W_9O_{40}$	3649, 3447, 3260, 2959, 2871, 1577, 1482, 1383, 1154, (**1086, 1048**),[c] 949, 885, 803, 646, 523
X $\alpha\text{-}1,2,3\text{-}Cs_6PV_3W_9O_{40}$	3652, 3475, 3181, 1639, (**1089, 1055**),[c] 956, 874, 792, 615, 520

[a] Characteristic doublet corresponding to the mono-vanadium substitution; intensity ratio 1:1. [b] Characteristic triplet corresponding to the di-vanadium substitution; intensity ratio 1:1:1. [c] Characteristic doublet corresponding to the tri-vanadium substitution; intensity ratio 2:1.

in the solution NMR spectra, in agreement with the symmetry of the vanadium sites in the Keggin anion.

In the solid state, the isotropic chemical shifts appear to be determined by the nature of the countercation. Mono- and tri-

Table 3. Experimental ^{51}V Solid-State and Solution NMR Parameters for the Vanadium-Substituted Keggin Oxotungstates **I–X**: ^{51}V Isotropic Chemical Shifts (δ_{Iso}), Quadrupolar Couplings (C_Q, η_Q), Chemical Shielding Anisotropies (δ_σ, η_σ), and the Euler Angles (α, β, γ), Describing the Relative Orientations of the Two Tensors

compd	C_Q, MHz 9.4 T (11.7 T)[a]	η_Q	δ_σ, ppm	η_σ	α, deg	β, deg	γ, deg	δ_{obsvd}, ppm (solid state)	quadrupole induced shift, ppm	δ_{iso}, ppm (solid state)	δ_{iso}, ppm (solution)
I K$_4$PVW$_{11}$O$_{40}$	0.94 ± 0.12	0.48 ± 0.19	536.6 ± 14.3	0.16 ± 0.15	0–180	64 ± 4	26 ± 17	−561.5	−0.2	−561.3	−557.3
	0.79 ± 0.09	(0.4 ± 0.14)	(531 ± 30)	(0.3 ± 0.15)		(60 ± 7)	(35 ± 15)				
II [(*n*-C$_4$H$_9$)$_4$N]$_4$PVW$_{11}$O$_{40}$	1.13 ± 0.03	0.61 ± 0.12	521 ± 40	0.13 ± 0.19	0–180	52 ± 9	42 ± 4	−543.3	−0.3	−543.0	−550.3
	(0.98 ± 0.03)	(0.5 ± 0.1)	(507 ± 10)	(0.15 ± 0.15)		(57 ± 8)	(41 ± 7)	−552.0		−551.7	
III Cs$_4$PVW$_{11}$O$_{40}$	1.25 ± 0.13	0.53 ± 0.21	589 ± 40	0.25 ± 0.06	0–180	55 ± 10	52 ± 3	−564.3	−0.4	−563.9	
	(1.25 ± 0.14)	(0.40 ± 0.28)	(551 ± 80)	(0.30 ± 0.42)		(65 ± 7)	(50 ± 5)				
IV [Na$_x$Cs$_{4-x}$]PVW$_{11}$O$_{40}$	1.15 ± 0.21	0.15 ± 0.21	590 ± 40	0 ± 0.05	0–180	62.5 ± 3.5	50	−562.7	−0.3	−562.4	
V α-1,2-H$_3$K$_2$[PV$_2$W$_{10}$O$_{40}$]· CH$_3$OH·14H$_2$O	1.79 ± 0.17	0.81 ± 0.26	516 ± 56	0.07 ± 0.16	0–180	62 ± 12	36 ± 3	−543.4	−0.9	−542.5	−548.5
	(1.80 ± 0.20)	(0.47 ± 0.06)	(494 ± 40)	(0.00 ± 0.05)		(55 ± 10)	(52 ± 3)				
VI α-1,2-[(*n*-C$_4$H$_9$)$_4$N]$_5$- PV$_2$W$_{10}$O$_4$	1.75 ± 0.08	0.77 ± 0.20	549 ± 19	0.01 ± 0.02	0–180	81 ± 12	39 ± 2	−557.8	−0.8	−557.0	−561.6
VII α-1,2-Cs$_5$PV$_2$W$_{10}$O$_{40}$	1.51 ± 0.19	0.57 ± 0.21	479 ± 33	0 ± 0.05	0–180	63 ± 6	42 ± 14	−533.7	−0.58	−533.12	
								−545.4			
VIII α-1,2,3-*K*$_6$PV$_3$W$_9$O$_{40}$	3.93 ± 0.06	0.87 ± 0.12	371 ± 34	0 ± 0	0–180	0 ± 0	38 ± 4	−526.6	−4.5	−522.1	533.62
								−538.2		−533.7	
IX α-1,2,3-[(*n*-C$_4$H$_9$)$_4$N]$_6$- PV$_3$W$_9$O$_{40}$	5.50 ± 0.71	0.75 ± 0.35	451 ± 34	0.05 ± 0.07	0–180	45 ± 63	40 ± 0	−452.7	−8.3	−444.4	562.73
								−480.3		−472	
X α-1,2,3-Cs$_6$PV$_3$W$_9$O$_{40}$	3.5 ± 0.08	1.0 ± 0.05	428 ± 20	0 ± 0.05	0–180	87 ± 6	5 ± 2	−523.7	−3.8	−519.9	
								−506.4		−502.6	

[a] Data in parentheses indicate measurements at 11.7 T (500 MHz).

vanadium substituted molecules show similar isotropic chemical shift dependence on the counterion. In **II** and **IV**, which are complexed with a TBA countercation vanadium atoms are more deshielded, with the isotropic chemical shifts of −543.0/−551.7 and −452.7/−480.3 ppm, respectively. The shifts of **I**, **III**, **IV**, which are mono-vanadium Keggin salts of alkali metals, are −561.3, −563.9, and −562.5 ppm. For the corresponding tri-vanadium Keggin derivatives **VIII** and **X**, the chemical shifts are −526.6/−538.2 and −523.7/−506.4 ppm. Interestingly, the di-vanadium derivatives exhibit the opposite countercation dependence, with the chemical shift for the TBA salt (**VI**) being more shielded (−557.0 ppm) than those for alkali metal salts **V** and **VII** (chemical shifts of −542.5 and −533.7/−545.4 ppm, respectively). To understand these trends, quantum mechanical calculations of magnetic shielding anisotropies will be required, using density functional theory and including the complete countercation environment. At present such calculations are not feasible because of the large number of heavy atoms and the overall size of the system.

Asymmetric spectral envelopes observed for all compounds indicate large chemical shielding anisotropies. The overall width of the spectral envelope reflects the magnitude of the quadrupolar interaction, and varies significantly as a function of the number of vanadium atoms in the Keggin anion, but appears to be only weakly dependent on the counterion. The quadrupole coupling constant increases with the number of vanadium atoms (mono- < di- < tri-), suggesting a more asymmetric charge distribution and very likely a more distorted geometric structure for the more substituted molecules.

Solid-State NMR Spectral Line Widths. The insets in Figures 3 and 4 contrast the line shapes for the individual spinning sidebands. The line widths range between 5.7 and 28.6 ppm. As anticipated, the narrowest lines (5.7 ppm) are observed for **II**, the mono-vanadium Keggin oxoanion prepared as a diffraction quality crystalline solid. The possible contributions to the line widths include the second-order quadrupolar broadening, the dipolar broadening, the positional disorder in vanadium distribution, and the bulk morphology of the solid.

The second-order quadrupolar broadening is expected to be weak in the mono-vanadium substituted **I–IV**, and become more pronounced for the di- and tri- vanadium compounds **V–X** due to the larger quadrupolar coupling constants. Indeed, the characteristic second-order quadrupolar line shape is observed both in the experimental and the simulated spectra for **V–X**.

Homonuclear ^{51}V–^{51}V dipolar coupling has a weak effect on the line widths for the Keggin solids. The V–V distance in the di- and tri- vanadium derivatives is 3.5 Å, and the corresponding dipolar coupling constant ω_D is 193 Hz. Additionally, as has been pointed out by S. Wimperis and colleagues previously,[42] in a dipolar-coupled system of two quadrupolar nuclei, such as a ^{51}V–^{51}V pair, a second-order quadrupolar-dipolar cross term is not averaged out by MAS, resulting in additional broadening of the spinning sidebands. However, since this term is scaled with the quadrupolar coupling strength,[42] its contribution to the line width is expected to be insignificant (of the order of 15–50 Hz) for the compounds discussed in this work.

The largest contributions to the line widths appear to arise from the positional disorder with respect to the vanadium atoms, and from the bulk morphology of the sample. Positional disorder is common in substituted polyoxometalates, and was revealed in the X-ray structures of **II**, **V**, and **VI**. This disorder causes spread in both the values of the quadrupolar coupling constant, and in the isotropic chemical shifts. For example, in the crystalline form of **II** two distinct sets of individual spinning sidebands were observed (Figure 3b) that most likely represent two different magnetically nonequivalent positions of vanadium sites in the crystalline lattice. In the samples prepared as powders, conformational heterogeneity introduces additional linebroadening, as is illustrated in the insets of Figure 3b, for crystalline and powder morphologies of **II**. Interestingly, doublet structure of the individual sidebands was observed for di- and tri-vanadium compounds (Figure 4), which also indicates presence

(42) McManus, J.; Kemp-Harper, R.; Wimperis, S. *Chem. Phys. Lett.* **1999**, *311*, 292–298.
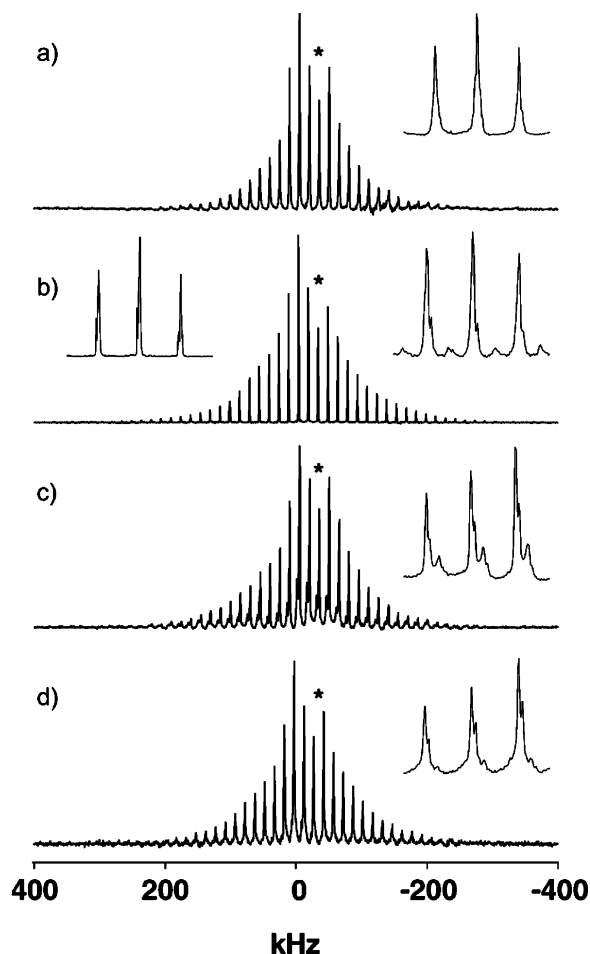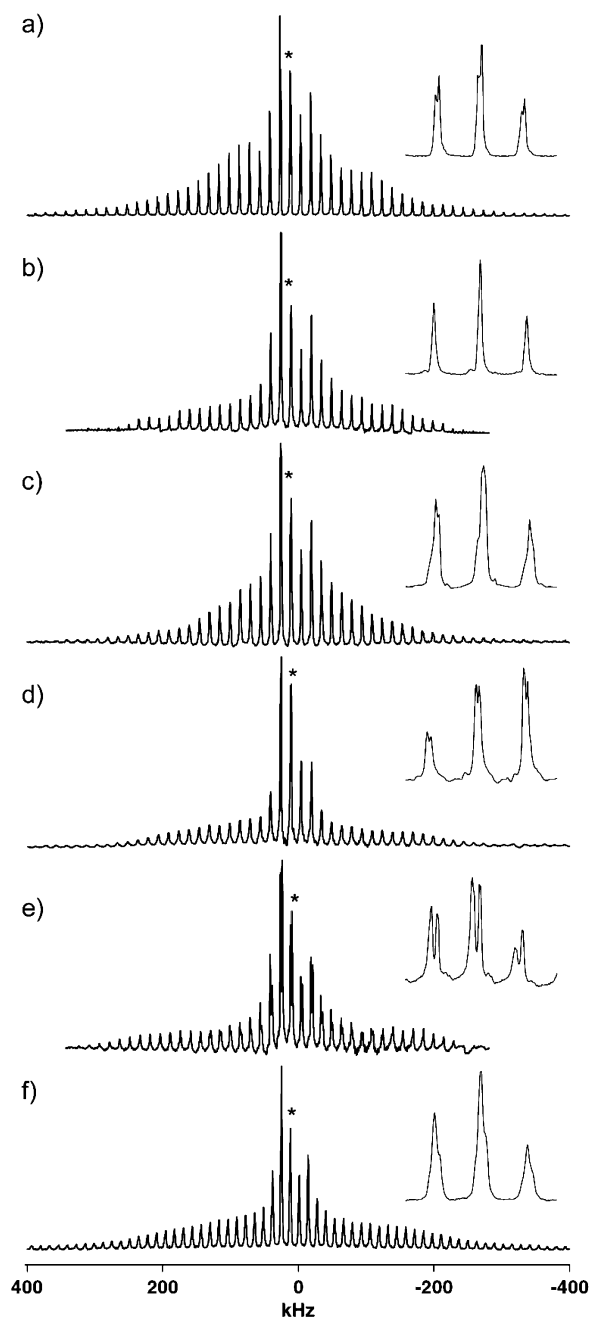
Figure 3. Experimental 9.7 T ^{51}V MAS NMR spectra of the mono-vanadium Keggin solids (a) **I** (crystal), (b) **II** (amorphous powder), (c) **III** (amorphous powder), (d) **IV** (amorphous powder), at 15 kHz. The center band is indicated with an asterisk. The isotropic chemical shifts are compiled in Table 3 with respect to neat VOCl$_3$, used as an external referencing standard. The insets on the right are expansions around the centerband to demonstrate the line shapes of the individual spinning sidebands. For **II**, the insets are shown for samples prepared both as diffraction quality crystals (left) and amorphous powder (right), to illustrate the two dominant sources of line broadening-positional disorder of vanadium in the crystalline lattice, and conformational heterogeneity.

of two magnetically nonequivalent vanadium positions in the crystal lattice rather than a random distribution of orientations.

Simulations of the Solid-State NMR spectra. The parameters describing the quadrupolar and CSA interactions were determined from numerical simulations of the solid-state NMR spectra, and are reported in Table 3 for each of the 10 compounds. The asymmetric line shapes in the MAS spectra result from the combined effect of the anisotropic quadrupolar and CSA interactions, and are described by seven independent parameters: the anisotropy and the asymmetry of the quadrupolar and CSA tensors (C_Q, η_Q, δ_σ, and η_σ), and the three Euler angles (α, β, and γ) relating the Principal Axes System (PAS) of the quadrupolar and CSA tensors. For ^{51}V and a number of other half-integer quadrupolar nuclei, the quadrupolar and CSA interactions are orders of magnitude different in strength, thus allowing for the seven independent parameters describing these interactions to be obtained from a single MAS spectrum.

We have acquired and simulated MAS spectra for each compound at five different spinning speeds, to be able to extract with greater accuracy the quadrupolar and CSA tensor elements,
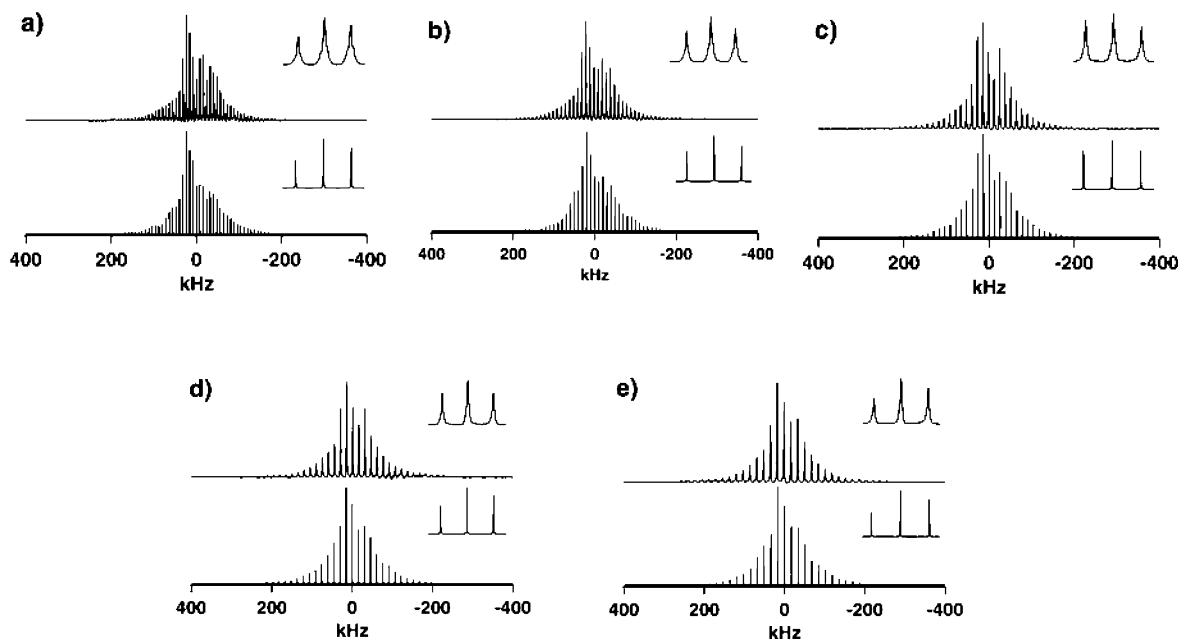

Figure 4. Experimental 9.7 T ^{51}V MAS NMR spectra of di- and tri-vanadium Keggin solids (a) **V**, (b) **VI**, (c) **VII**, (d) **VIII**, (e) **IX**, (f) **X** at 15 kHz. The center band is indicated with an asterisk. The isotropic chemical shifts are compiled in Table 3 with respect to neat VOCl$_3$, used as an external referencing standard. The insets are expansions around the centerband to demonstrate the line shapes of the individual spinning sidebands.

and to obtain reliable error estimates. The anisotropic observables were found to be consistent at all spinning speeds. For **I**, **II**, **III**, **V**, and **VI**, the spectra were also acquired at two magnetic field strengths, 9.7 and 11.4 T, and the results are in good agreement. In Figures 5−7, the experimental and simulated spectra at several spinning speeds are shown for representatives of mono-, di-, and tri-vanadium series, **I**, **V**, and **VIII**.

Effect of Cationic Environment and Vanadium Substitution on Quadrupolar and CSA Tensors. The experimental data discussed above reveal that in Keggin solids, both counter-cations and vanadium substitution determine the anisotropic
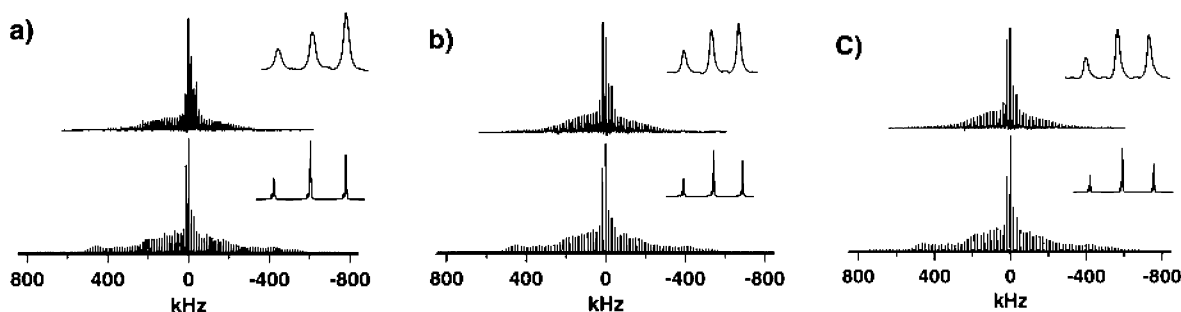
Figure 5. Experimental (top) and simulated (bottom) ^{51}V MAS NMR spectra of α-K$_4$[PVW$_{11}$O$_{40}$] (**I**) at (a) 7.986 kHz, (b) 10.000 kHz, (c) 13.010 kHz, (d) 15.190 kHz, and (e) 16.980 kHz. The spectra were simulated using the following parameters: $C_Q = 0.94 \pm 0.12$ MHz; $\delta_\sigma = 536.6 \pm 14.3$ ppm; $\eta_Q = 0.48 \pm 0.19$; $\eta_\sigma = 0.16 \pm 0.15$; α = undetermined; $\beta = 64 \pm 4°$; $\gamma = 26 \pm 17°$. The rmsd values were (a) 0.08, (b) 0.08, (c) 0.07, (d) 0.06, and (e) 0.05. The insets are expansions of a satellite peak comparing the experimental and simulated line shapes of the individual spinning sidebands.
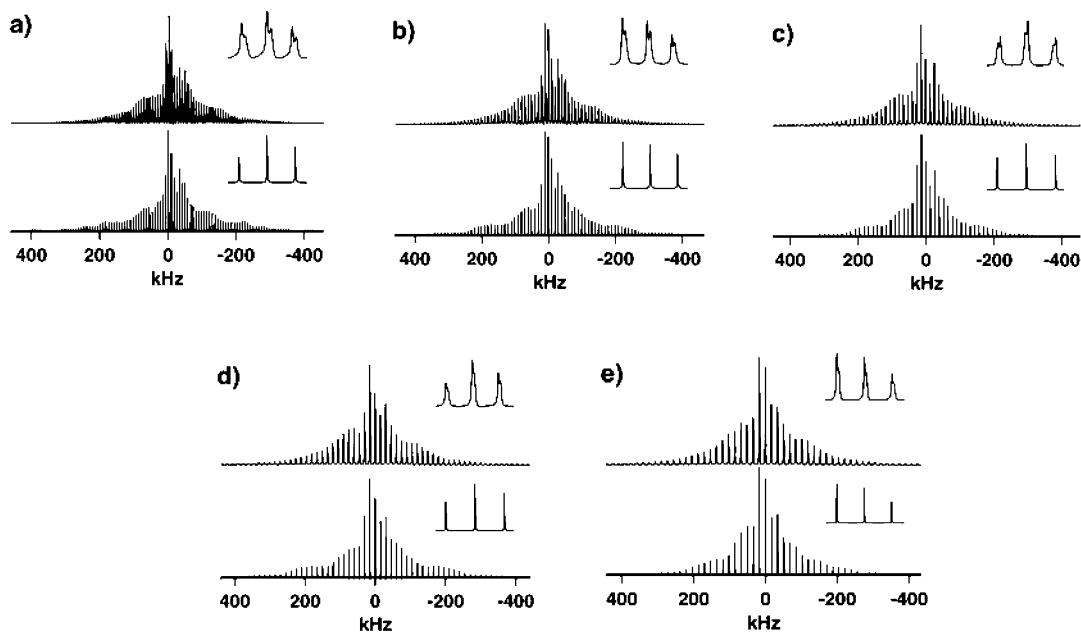
Figure 6. Experimental (top) and simulated (bottom) ^{51}V MAS NMR spectra of α-1,2-K$_2$H$_3$[PV$_2$W$_{10}$O$_{40}$]·2CH$_3$OH·7H$_2$O (**V**) at (a) 8.000 kHz, (b) 10.011 kHz, (c) 13.010 kHz, (d) 15.000 kHz, and (e) 17.000 kHz. The spectra were simulated using the following parameters: $C_Q = 1.79 \pm 0.17$ MHz; $\delta_\sigma = 516 \pm 56$ ppm; $\eta_Q = 0.81 \pm 0.26$; $\eta_\sigma = 0.07 \pm 0.16$; α = undetermined; $\beta = 62 \pm 12°$; $\gamma = 36 \pm 3°$. The rmsd values were (a) 0.08, (b) 0.08, (c) 0.06, (d) 0.08, and (e) 0.06. The insets are expansions of a satellite peak comparing the experimental and simulated line shapes of the individual spinning sidebands.

NMR observables (C_Q, δ_{iso}, and δ_σ). Interestingly, and somewhat unexpectedly, in the Keggin series under investigation, countercations have large effect on the chemical-shielding anisotropy tensor components, but only weakly influence the quadrupolar interaction. For comparison, in Lindqvist polyoxometalates, the quadrupolar interaction is dictated by counteractions,[40] which determine the crystal packing and the symmetry of electronic charge distribution. In Keggin solids, the weak countercation influence can be qualitatively understood by analysis of crystal structures of **II**, **V**, and **VI** in the following way. According to the classical point monopole model, the electric field gradient

is treated in purely electrostatic terms, and its matrix is represented by the nine entries $V_{ij} = ne(3ij/r^5 - \delta_{ij}/r^3)$, where e is the electronic charge, ne is the charge on each atom, i and j are the Cartesian x, y, or z coordinates of the ligand atom (assuming the coordinates of the central vanadium are (0, 0, 0)), and r is the distance between the ligand and the central vanadium atom. The contribution of the individual charge scales linearly with its magnitude and as the cube of the distance to the central atom. In practice, this contribution is negligible for distances of 4 Å and longer. According to the X-ray structure of **V**, the shortest distance between the K$^+$ cation and the

Figure 7. Experimental (top) and simulated (bottom) ^{51}V MAS NMR spectra of α-1,2,3-$K_6[PV_3W_{10}O_{40}]$ (**VIII**) at (a) 13.199 kHz, (b) 15.213 kHz, and (c) 17.239 kHz. The spectra were simulated using the following parameters: $C_Q = 3.93 \pm 0.06$ MHz; $\delta_\sigma = 371 \pm 34$ ppm; $\eta_Q = 0.87 \pm 0.12$; $\eta_\sigma = 0 \pm 0$; α = undetermined; $\beta = 0 \pm 0°$; $\gamma = 38 \pm 4°$. The rmsd values were (a) 0.12, (b) 0.08, and (c) 0.07. The insets are expansions of a satellite peak comparing the experimental and simulated line shapes of the individual spinning sidebands.

vanadium atom in the Keggin anion is 4.18 Å; the distances from vanadium to protons of the hydration water molecules are somewhat shorter (ca., 3.8−4.0 Å), but due to the overall electrical neutrality of water molecules, their contribution to the electric field gradient at these distances is expected to be small. In **II** and **VI**, the shortest distance from vanadium to one of the hydrogen atoms on the $[(n\text{-}C_4H_9)_4N]^+$ cations is 3.3 Å; the shortest possible distance to a carbon atom in $[(n\text{-}C_4H_9)_4N]^+$ is 4.2 Å, and that to nitrogen is 5 Å. Thus, the only possible contribution to the EFG tensor could come from a hydrogen atom on $[(n\text{-}C_4H_9)_4N]^+$. However, based on the density functional theory calculations, the partial atomic charges on the hydrogen atoms do not exceed +0.22 (natural charge) or +0.19 (Mulliken charges), and their effect on the overall EFG tensor will be very small even at 3.3 Å. The natural and Mulliken charges are given in Table 1s of the Supporting Information.

Despite the fact that no X-ray structures are available for Na^+ and Cs^+ salts, very mild variations in the quadrupolar interaction parameters suggest similar cationic environment, i.e., relatively large vanadium-to-cation distances. In comparison, the average metal to Na^+ cation distances were found to be significantly shorter (of the order of 3.6 Å) in vanadium-substituted Lindqvist hexametalates, where the quadrupolar coupling constants were dictated by the countercations.[40]

In contrast, ^{51}V chemical shielding anisotropies were found to be very sensitive to the countercations in **I−X** (Table 3). Most likely, this is an indirect effect involving terminal oxygen atoms, which are at relatively short distances to alkali metals and $[(n\text{-}C_4H_9)_4N]^+$. For example, in **V** the K^+-to-terminal O distance is 2.7 Å, and strong electrostatic interactions are expected, which are likely to modulate the electronic structure of the entire anion. For a more rigorous understanding of the countercation effect on chemical shielding anisotropy in the Keggin solids, a quantum mechanical treatment is required, which will be the subject of a separate study.

Conclusions

The work reported here demonstrates that ^{51}V solid-state MAS NMR spectroscopy can be used as a sensitive probe of the cationic environment, vanadium substitution, positional disorder, and bulk morphology of Keggin oxotungstate solids. The quadrupolar interaction in these solids is determined mostly by the number of vanadium atoms in the oxotungstate anion core. The chemical-shielding anisotropy tensor is affected by the

nature and geometry of countercations, as well as vanadium substitution. The multiplet structure in the individual spinning sidebands reflects the positional disorder with respect to vanadium atoms. The line widths report on sample morphology. Thus, a single ^{51}V MAS NMR spectrum provides a quick, convenient, and nondestructive probe of the above molecular properties. That the chemical-shielding anisotropy tensor elements are dictated by the countercation environment in each series of mono-, di-, and tri-vanadium substituted compounds suggests that the electronic structure of the entire Keggin anion is modulated by the crystal field. Similarly, the electronic structure of the anion depends on the number of vanadium atoms in the anion molecule, as is manifested by the pronounced effect of vanadium substitution on the CSA and the quadrupolar anisotropy tensors. These results suggest that the previously observed dependence of chemical reactivities and thermal stabilities of Keggin oxotungstate catalysts on countercation and vanadium substitution, could result from the altered electronic environment.[9,10] ^{51}V Magic Angle Spinning NMR spectroscopy thus exhibits excellent promise to become a widely utilized tool for the analysis of oxoanionic Keggin solids, as well as for design of Keggin materials with tunable catalytic properties.

Supporting Information Available: Crystallographic coordinates for **II**, **V**, and **VI**; a figure showing calculated ^{51}V NMR spectra for a hypothetical $^{51}V(V)$ diamagnetic solid; a table of Mulliken and natural charges for $[(n\text{-}C_4H_9)_4N]^+$ calculated using density functional theory implemented in Gaussian98 (CIF, PDF). This material is available free of charge via the Internet at http://pubs.acs.org.

JA0475499